

Attenuation Relationships of Peak Ground Acceleration and Velocity for Crustal Earthquakes in Taiwan

by Kun-Sung Liu and Yi-Ben Tsai

Abstract Strong seismic ground-motion data obtained by the Taiwan Strong Motion Instrumentation Program (TSMIP) and Central Mountain Strong Motion Array (CMSMA) are used to derive new attenuation relationships for the vertical and horizontal peak ground acceleration (PGA) and peak ground velocity (PGV) for crustal earthquakes in Taiwan. More than 7900 three-component accelerograms recorded from 51 crustal earthquakes in Taiwan, with M_w magnitudes ranging from 4.0 to 7.1, have been analyzed to study the dependence of peak ground motion parameters on magnitude, distance, regional and local site effects, through attenuation relationships.

We first found that, for both PGA and PGV, the attenuation relationships decay faster with distance for the vertical component than for the horizontal component. Also, the attenuation relationships decay faster with distance for the vertical PGA than for the vertical PGV. We further compared the attenuation relationships for three subregions (CHY, IWA, and NTO) and the whole Taiwan region (TWN). It is found that the CHY area has higher ground motion, either in PGA or PGV, than the other areas, especially at near-source distances. This is because the CHY area is located on a thick, recent alluvial plain. Comparison of our new attenuation relationships with strong-motion data from the 1999 Chi-Chi earthquake (M_w 7.7) and the 2003 Cheng-Kung earthquake (M_w 6.8) shows that the attenuation relationships developed for $M_w \leq 7$ can be extrapolated to make reasonable estimates of strong motion from larger $M_w \geq 7$ earthquakes. Finally, we analyzed the residuals to investigate variations of PGA and PGV with respect to site conditions. The results show that (1) the residual contour maps, especially for the PGV, have high consistency with the regional geology and topography of Taiwan. (2) The PGV residual contours reveal that Taipei Basin, Changhua Plain, Chianan Plain, Pingtung Valley, Ilan Plain, and Taitung Longitudinal Valley have high residual values. Note that most major metropolitan areas all fall in high residual areas. (3) The site classification based on geologic criteria by Lee *et al.* (2001) can be simplified into three classes, that is, class E for soft soils, a combination of classes C and D for dense and stiff soils, and class B for rocks. These three site classes are mostly distributed, respectively, in the alluvial plains at an elevation less than 50 m, in terraces and hills at an elevation less than 1000 m, and in high mountainous areas.

Introduction

Well-documented assessment of seismic hazards is a fundamental step in the process of earthquake disaster mitigation. Seismic hazard assessment requires ground-motion attenuation models. Estimates of expected ground motion at a given site from earthquakes of different magnitudes and distances are fundamental input to earthquake hazard assessment. These estimates are usually obtained from equations, called attenuation relationships, that express ground-motion parameter values as a function of magnitude and

distance (and, in some cases, other variables, such as site condition and style of faulting).

Beginning in 1991, the Seismology Center of Central Weather Bureau (CWBS) embarked on a six-year seismic strong-motion instrumentation program, known as the Taiwan Strong Motion Instrumentation Program (TSMIP) (Shin, 1993). The main goal of this program is to collect high-quality instrumental recordings of strong earthquake shaking. These data are crucial for improving the earthquake-

resistant design of buildings and for understanding earthquake source mechanisms, and seismic wave propagation from the source to the site of interest, including local site effects. By now, more than 650 stations have been deployed and more than ten thousand high-quality digital accelerograms have been collected. These new recordings provide an excellent database for making attenuation relationship studies, (Liu, 1999; Chang *et al.*, 2001; Wu *et al.*, 2001).

This study describes a set of empirical attenuation relationships that were specifically developed to predict horizontal and vertical components of peak ground acceleration (PGA) and peak ground velocity (PGV) for crustal earthquakes in the Taiwan region. The results are analyzed to investigate the variations of attenuation relationships with magnitude, distance, and regional and local site effects.

Strong-Motion Data

Strong seismic ground-motion data obtained by the TSMIP and the Central Mountain Strong Motion Array (CMSMA) (www.earth.sinica.edu.tw/~smdmc/cma/cma.htm) are used to derive new attenuation relationships. The TSMIP is designed to enhance our ability to monitor strong earthquakes and to collect high-quality instrumental recordings of strong earthquake shaking. The selection criteria for the TSMIP accelerograph sites are set as follows: (1) in nine major metropolitan areas; (2) near known fault zones; (3) at different geological sites: rock, medium-stiff soil, and soft soil; (4) near important construction or industrial sites or nuclear power plants (Liu *et al.*, 1999).

The TSMIP accelerograph network currently consists of more than 650 free-field stations. The locations of these stations are shown in Figure 1. Except in the mountainous areas, these free-field stations are densely spaced approximately 5 km apart, but only about 3 km apart in urban areas (as compared with a 25-km uniform spacing of the K-Net in Japan).

The deployment of these instruments started in August 1992 with most being operational by December 1994. Each operating free-field station includes triaxial accelerometers, a digital recording subunit, a power supply, and a timing system. To handle the large work load to maintain so many free-field stations located all over Taiwan, the CWBSC has enlisted the help of the Institute of Earth Sciences at Academia Sinica, the Institute of Geophysics at National Central University, and the Institute of Seismology at National Chung-Cheng University to collect the recorded data.

The primary purpose of the TSMIP accelerographs is to record moderate to large earthquakes at distances and locations of major scientific and societal significance. Attention is also given to collecting data from more frequent small earthquakes.

Taking into account the relatively low likelihood of large earthquakes, the unpredictability in the location and time of these events, and the societal significance of the re-

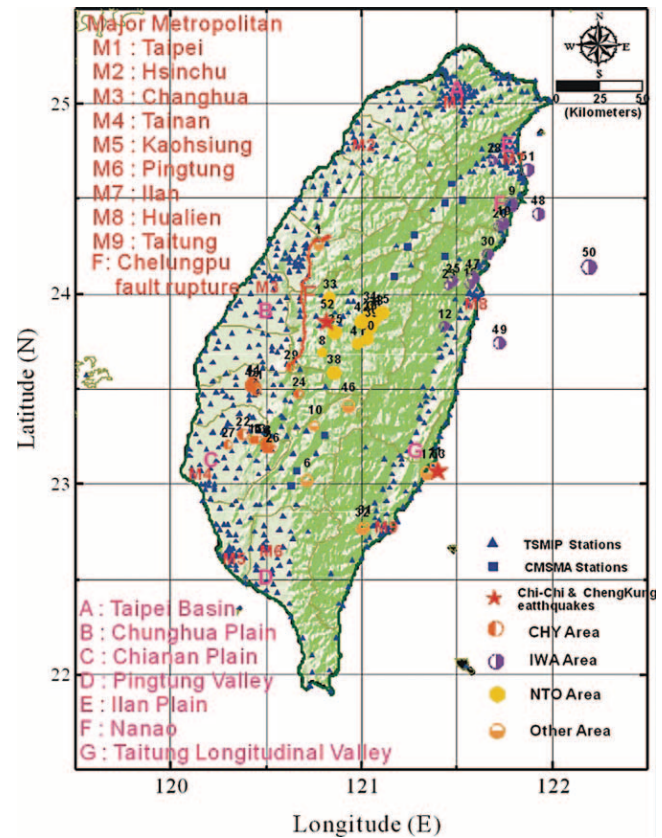


Figure 1. Distribution of the TSMIP and CMSMA free-field stations and the epicenters of earthquakes used in this study. The filled triangle and filled square represent the TSMIP and CMSMA stations, respectively. The orange, purple, and yellow circles mark the earthquakes of the CHY, IWA, and NTO subregions, respectively. The number above each earthquake corresponds to the index in Table 1. The Chi-Chi mainshock epicenter (event 52), Cheng-Kung earthquake (event 53), the Chelungpu fault rupture, main localities, and topography are also indicated.

corded data, stringent engineering and scientific requirements for the accelerograph are set.

The transducers for the accelerograph must respond accurately in the frequency range from direct current (DC) to 50 Hz to record faithfully the near-source ground motion caused by large earthquakes. To record a wide range of earthquakes on scale, the complete system must be digital and have at least a 16-bit resolution (Liu *et al.*, 1993).

More than ten thousand high-quality digital accelerograms have already been collected by the TSMIP from more than 6000 earthquakes. These new recordings provide an excellent database for making various earthquake engineering and seismological studies. In addition to the TSMIP data, similar CMSMA instrumentation was installed by Academia Sinica in the Central Mountain areas, which suffer from severe lack of strong-motion data.

More than 7900 digital accelerograms recorded from 51 crustal earthquakes, by the TSMIP and CMSMA instruments,

as given in Table 1 and shown in Figure 1, were selected for this study. The M_w magnitudes range from 4.0 to 7.1. These records are analyzed to investigate the dependence of attenuation relationships on magnitude, regional clustering of sources, and site effects. The earthquakes of event numbers 1 to 32 were relocated by Wu *et al.* (1998) according

to the following criteria: (1) The focal depths were less than 30 km, and (2) at least six stations recorded the events at an epicentral distance less than 20 km.

In addition, large and shallow earthquakes often cause serious damage in heavily populated areas, so we selected earthquakes of event numbers 33 to 51 with a local magni-

Table 1
Earthquakes Whose Records Are Used in the Regression Analysis

No.	Date (yy/mm/dd)	Time	Latitude (N)	Longitude (E)	Depth (km)	rms (sec)	ERH (km)	ERZ (km)	M_L	M_w	Recording No.
1	93/12/13	09:23:00.00	24.256	120.776	25.75	0.09	4.7	0.6	4.53	4.37	28
2	93/12/15	21:49:43.10	23.194	120.507	15.21	0.12	0.4	0.2	5.70	5.40*	138
3	93/12/20	03:32:04.58	23.227	120.506	17.13	0.10	0.4	0.3	4.41	4.25	39
4	93/12/21	03:14:28.54	23.216	120.509	18.58	0.09	0.5	0.4	4.49	4.33	42
5	93/12/22	16:22:20.00	23.208	120.499	17.42	0.13	0.6	0.2	4.63	4.47	44
6	94/03/28	08:11:15.71	23.018	120.714	23.09	0.19	0.5	0.4	5.41	5.25	81
7	94/04/06	01:12:11.09	23.494	120.448	18.97	0.14	0.1	0.1	5.03	4.87	76
8	94/05/31	15:00:06.07	23.692	120.794	9.18	0.13	0.2	0.5	4.57	4.41	35
9	94/06/05	01:09:30.09	24.468	121.787	5.13	0.09	0.5	0.5	6.50	6.40*	214
10	95/01/19	11:39:08.60	23.305	120.753	17.01	0.15	0.5	0.4	4.46	4.30	45
11	95/02/26	08:08:18.46	23.088	121.384	19.86	0.14	1.1	0.4	4.87	4.71	39
12	95/03/22	03:30:21.65	23.831	121.435	7.44	0.12	0.7	0.3	4.84	4.68	34
13	95/04/23	02:47:40.17	23.233	120.459	11.86	0.11	0.6	0.2	4.25	4.09	33
14	95/04/23	02:57:52.32	23.233	120.437	9.80	0.18	0.9	0.3	4.32	4.16	40
15	95/04/23	03:01:46.30	23.234	120.441	12.09	0.09	0.5	0.1	4.31	4.15	45
16	95/05/01	14:50:45.67	24.052	121.569	12.99	0.07	0.8	0.2	4.89	4.73	30
17	95/05/27	18:11:11.12	23.058	121.342	21.05	0.12	1.0	0.3	5.26	5.70*	143
18	95/07/07	03:04:48.36	23.896	121.078	15.19	0.13	0.5	0.4	5.30	5.14	163
19	95/07/14	16:52:46.48	24.368	121.743	9.83	0.13	1.0	0.3	5.80	5.65*	194
20	95/07/14	17:40:48.42	24.358	121.719	5.24	0.13	1.0	0.6	4.87	4.71	31
21	95/09/28	17:58:05.32	23.509	120.449	11.93	0.17	0.9	0.2	4.48	4.32	54
22	95/10/31	22:27:06.94	23.262	120.380	18.51	0.11	0.1	0.1	5.19	5.03	117
23	95/11/14	07:26:26.68	24.044	121.456	10.32	0.12	0.1	0.1	4.21	4.05	28
24	96/04/07	16:55:36.26	23.475	120.670	4.44	0.12	1.7	1.0	4.70	4.54	45
25	96/05/28	21:53:22.35	24.069	121.477	16.21	0.10	0.6	0.3	5.05	4.89	71
26	96/10/19	19:16:05.11	23.183	120.532	16.88	0.22	0.5	0.2	4.21	4.05	41
27	96/11/16	00:22:43.64	23.208	120.300	20.23	0.09	0.8	0.2	4.28	4.12	35
28	97/04/02	22:36:41.85	24.701	121.692	8.48	0.14	0.3	0.1	4.33	4.17	48
29	97/10/29	23:18:37.39	23.618	120.628	13.32	0.10	0.3	0.1	4.32	4.16	33
30	97/11/14	04:29:50.77	24.209	121.662	10.22	0.07	0.8	0.2	5.40	5.24	53
31	98/01/18	19:56:51.71	22.773	121.015	3.34	0.08	0.1	0.1	5.07	4.91	54
32	98/01/20	23:29:38.87	22.763	121.003	2.72	0.15	0.1	0.1	5.07	4.91	34
33	99/09/20	17:49:40.07	23.977	120.830	19.74	0.15	1.6	1.1	6.07	5.92	127
34	99/09/20	17:57:15.58	23.912	121.044	7.68	0.30	0.4	0.5	6.44	6.29	326
35	99/09/20	18:03:41.57	23.797	120.861	9.75	0.37	0.8	0.7	6.60	6.45	324
36	99/09/20	18:11:54.21	23.865	121.067	12.49	0.48	0.9	0.9	6.70	6.55	374
37	99/09/20	18:16:17.95	23.862	121.041	12.53	0.30	0.6	0.5	6.66	6.51	366
38	99/09/20	21:46:38.11	23.585	120.857	8.57	0.21	0.5	0.5	6.59	6.40*	336
39	99/09/22	00:14:40.77	23.826	121.047	15.59	0.23	0.5	1.1	6.80	6.40*	353
40	99/09/22	00:49:43.45	23.765	121.031	17.38	0.31	0.7	1.4	6.20	5.80*	320
41	99/09/22	12:17:20.96	23.739	120.981	24.02	0.25	0.5	0.5	6.00	5.30*	204
42	99/09/25	23:52:49.63	23.854	121.002	12.06	0.28	0.6	1.9	6.80	6.50*	358
43	99/10/22	02:18:56.90	23.517	120.423	16.59	0.29	0.7	0.6	6.40	5.90*	335
44	99/10/22	03:10:17.46	23.533	120.431	16.74	0.24	0.5	0.6	6.00	5.60*	274
45	00/06/10	18:23:29.45	23.901	121.109	16.21	0.30	0.6	0.9	6.70	6.40*	414
46	00/07/28	20:28:07.72	23.411	120.933	7.35	0.38	0.4	0.6	6.10	5.70*	258
47	00/09/10	08:54:46.53	24.085	121.584	17.74	0.17	0.5	0.4	6.20	5.80*	211
48	01/06/14	02:35:25.78	24.419	121.928	17.29	0.34	1.3	0.9	6.30	5.90*	261
49	02/02/12	03:27:25.00	23.741	121.723	29.98	0.44	1.2	0.8	6.20	5.70*	369
50	02/03/31	06:52:49.95	24.140	122.192	13.81	0.32	2.1	2.2	6.80	7.10*	382
51	02/05/15	03:46:05.91	24.651	121.872	8.52	0.38	0.8	0.6	6.20	6.20*	208

*The moment magnitude (M_w) adopted from the Harvard CMT.

tude greater than 6 after the Chi-Chi earthquake of 20 September 1999 (UTC). In this study, we did not include the data of 1999 M_w 7.7 Chi-Chi and 2003 M_w 6.8 Cheng-Kung earthquakes in the main regression analysis because of the following considerations. (1) A preliminary analysis of the ground-motion data from the Chi-Chi earthquake indicated that the median short-period ground motion was significantly lower than that predicted from contemporary attenuation relationships (Tsai and Huang, 2000; Boore, 2001; Campbell and Bozorgnia, 2003). (2) The powerful dynamic rupturing process of the Chelungpu fault apparently triggered two M 6 events, each one having occurred in the vicinity of a known fault: one off the southern end and the other off the northern end of the Chelungpu fault (Shin and Teng, 2001). The ground motion caused by these events could have contaminated the accelerograms of some nearby stations so that the PGA and PGV values were not caused solely by the main shock of Chi-Chi earthquake. (3) The digital accelerograms of the Cheng-Kung earthquake were not yet available when our regression analysis was made. Instead, we used the data of these two earthquakes to test the applicability of extrapolating our regression results for larger earthquakes.

In this study, the earthquakes are characterized by their moment magnitude (M_w). In the CWB earthquake catalog, all events are given a local magnitude, which normally saturates at a value of about 6.5 (Heaton *et al.*, 1986; Reiter, 1991). Therefore, we have adopted the moment magnitude from the Harvard centroid moment tensor (CMT) database (asterisk in Table 1). And for other earthquakes that were not reported by Harvard CMT mostly smaller than M_w 5.3, we used the following empirical equation (Y. B. Tsai and K. P. Chen, unpublished manuscript, 1998) to convert the M_L to M_w :

$$M_L = 0.193 + 0.993 M_w \quad (1)$$

where M_L is the local magnitude and M_w is the moment magnitude, respectively.

For PGA and PGV values we use the vertical and mean of the two horizontal components. We derive the attenuation relationships for three regions and for the whole Taiwan area to compare the regional difference of source clustering in ground-motion characteristics. The three regions are the CHY area in southwestern Taiwan, including events 2, 3, 4, 5, 7, 13, 14, 15, 21, 22, 24, 26, 27, 29, 43, and 44; the IWA area in northeastern Taiwan, including events 9, 12, 16, 19, 20, 23, 25, 28, 30, 47, 48, 49, 50, and 51; and the NTO area in central Taiwan, the same area as the Chi-Chi earthquake, including events 8, 18, 33, 34, 35, 36, 37, 38, 39, 40, 41, 42, and 45, respectively. Figure 1 shows the epicenters of these events by using different symbols for the three source regions. Figure 2 shows the data distribution of these events in terms of magnitude and hypocenter distance. The numbers of accelerograms used to derive the attenuation relationships for the three regional source areas CHY, IWA, and NTO are 1382, 2105, and 3671, respectively.

Development of the PGA and PGV Attenuation Relationships

The strong-motion attenuation relationships express earthquake ground-motion parameters as functions of simple parameters characterizing the earthquake source, the propagation path between the earthquake source and the site, and the geologic conditions beneath the site. The following equation form is used in this study:

$$\ln Y = a \ln(X + h) + b X + c M_w + d \pm \sigma \quad (2)$$

where Y is the ground-motion parameter, X is the hypocentral distance, M_w is the moment magnitude, a is the geometrical spreading coefficient, b is the anelastic attenuation coefficient, c is the magnitude coefficient, d is a constant, h is the close-in distance saturation coefficient, and σ is the standard deviation. The coefficients a , b , c , d , and h are to be determined by regression from the data (Liu, 1999). This equation form is similar to the one used by Joyner and Boore (1981), except for the difference in distance definitions.

We characterize the earthquake size by moment magnitude, M_w , as defined by Hanks and Kanamori (1979). We prefer M_w to surface-wave magnitude or local magnitude, because M_w corresponds to well-defined physical properties of the source. Furthermore, the rate of occurrence of earthquakes with different M_w values can be related directly to the slip rate on faults (Joyner and Boore, 1981). The use of moment magnitude avoids the "saturation" of the more traditional band-limited magnitude measures at large seismic moments and, therefore, is considered to be a better measure of the true size of an earthquake (Campbell, 1997).

Hypocentral distance is taken to represent source-to-site distance in this study. Focal depth and epicentral location of earlier events were relocated by Wu *et al.* (1998) combining data from the regional seismic network plus the TSMIP network operated by CWBSC. Inadequate information is available for the selected events to clearly define or compute the closest distance to the rupture zone, as defined by Boore *et al.* (1980) and Campbell (1981). Although a strong physical justification for such a distance definition may exist, it requires exact knowledge of the multiparametered source geometry, not known here with sufficient certainty for all the events (Niazi and Bozorgnia, 1991). In particular, for many of the smaller magnitude events, the rupture surface has not been defined. Moreover, because the dimensions of the rupture surface for small events are usually much smaller than the distances to the recording stations, we believe that the use of hypocentral distance will not introduce significant bias into the attenuation relationships (Sadigh *et al.*, 1997).

Another reason we chose hypocentral distance to represent source-to-site distance is that, during a disastrous earthquake, early assessment and timely reporting of the PGA and PGV maps will be crucial for effective emergency-response operations. Thus, with hypocentral distances being quickly determined right after the earthquake, we can com-

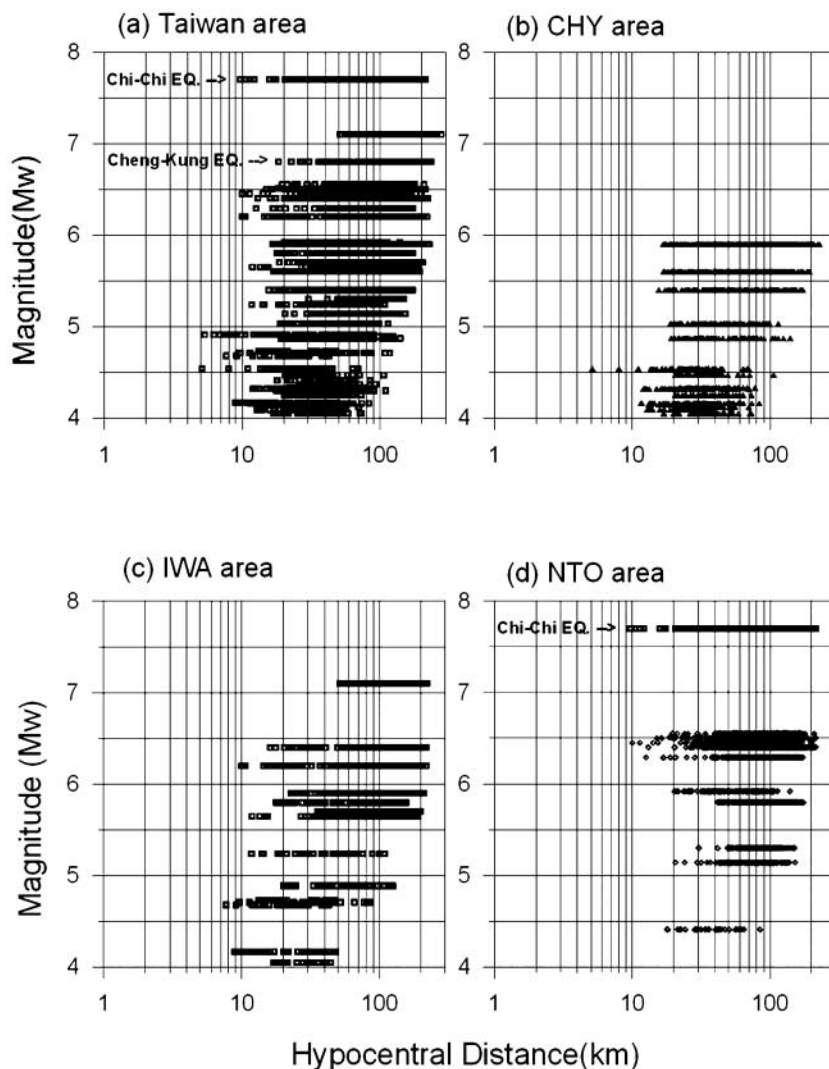


Figure 2. Distribution of strong-motion data used in this study to develop the attenuation relationships. (a) Taiwan area; (b) CHY area; (c) IWA area; (d) NTO area. The data from the Chi-Chi and Cheng-Kung earthquakes were not used in the main regression analysis but were used to test the regression results.

bine these attenuation relationships and local site residuals in near real-time to estimate and report the PGA and PGV values, in particular, for sites in metropolitan areas.

The coefficients in the equation for predicting ground motion were determined using a two-stage regression procedure (Liu, 1999). A similar approach was used previously by Joyner and Boore (1993). In the first stage, the distance-dependence coefficients a and b were determined along with a set of amplitude factors, one for each earthquake. In the second stage, the amplitude factors were regressed against magnitude to determine the magnitude-dependence coefficient c and the constant d .

Attenuation Relationships for Vertical and Horizontal PGA and PGV

Regressions on the data set without differentiating site conditions have resulted in the coefficients of the attenuation relationships, as given in Table 2, for the vertical (V) and horizontal (H) components of PGA and PGV for the whole

Taiwan region and the three subregions. In Table 2, σ refers to the standard deviation on $\ln(Y)$. Assuming a log-normal distribution, this value can be used to obtain the value of the parameter Y corresponding to different probability levels. Specifically, $\ln(Y)$ at 84% probability (mean plus one sigma) may be obtained by multiplying the predicted median value by e^σ .

Figure 3 plots the predicted mean values of the vertical and horizontal PGA as a function of distance for the whole Taiwan area. The solid lines represent the median predictions at hypocentral distance ranging from 10 to 279 km for M_w 4.0, 4.5, 5.0, 5.5, 6.0, 6.5, and 7.0, which are constrained by data, whereas the dashed lines represent the median predictions for M_w 7.5 and 8.0, by extrapolation. From the figure, we can find faster PGA attenuation for the vertical than the horizontal component. Figure 4 plots the predicted mean values of the vertical and horizontal PGV as a function of distance for the whole Taiwan area. The solid and dashed lines represent the same meanings as in Figure 3. From the figure, we can also find faster attenuation for the vertical than horizontal PGV.

Table 2
Regression Coefficients for PGA and PGV

Area		V Component						H Component					
		a	b	c	d	h	σ	a	b	c	d	h	σ
TWN	PGA	-1.340	-0.0036	1.101	1.697	1.62	0.687	-0.852	-0.0071	1.027	1.062	1.24	0.719
	PGV	-0.935	-0.0012	1.534	-5.273	1.19	0.604	-0.857	-0.0023	1.486	-4.472	1.34	0.711
CHY	PGA	-1.577	-0.0036	1.472	0.923	1.26	0.637	-1.322	-0.0071	1.445	0.979	0.96	0.638
	PGV	-1.147	-0.0012	1.653	-5.010	0.45	0.525	-1.412	-0.0023	1.825	-3.886	0.88	0.577
IWA	PGA	-1.188	-0.0036	1.049	1.370	1.24	0.703	-0.708	-0.0071	0.964	0.781	0.18	0.709
	PGV	-0.792	-0.0017	1.466	-5.535	0.37	0.573	-0.768	-0.0023	1.525	-5.151	0.21	0.700
NTO	PGA	-1.162	-0.0073	1.112	1.209	2.64	0.685	-0.898	-0.0074	1.030	1.287	3.48	0.725
	PGV	-0.981	-0.0012	1.512	-4.855	4.07	0.605	-0.839	-0.0023	1.385	-3.889	4.86	0.679

Attenuation model $\ln(\text{PGA,PGV}) = a*\ln(X + h) + b*X + c*M_w + d \pm \sigma$.

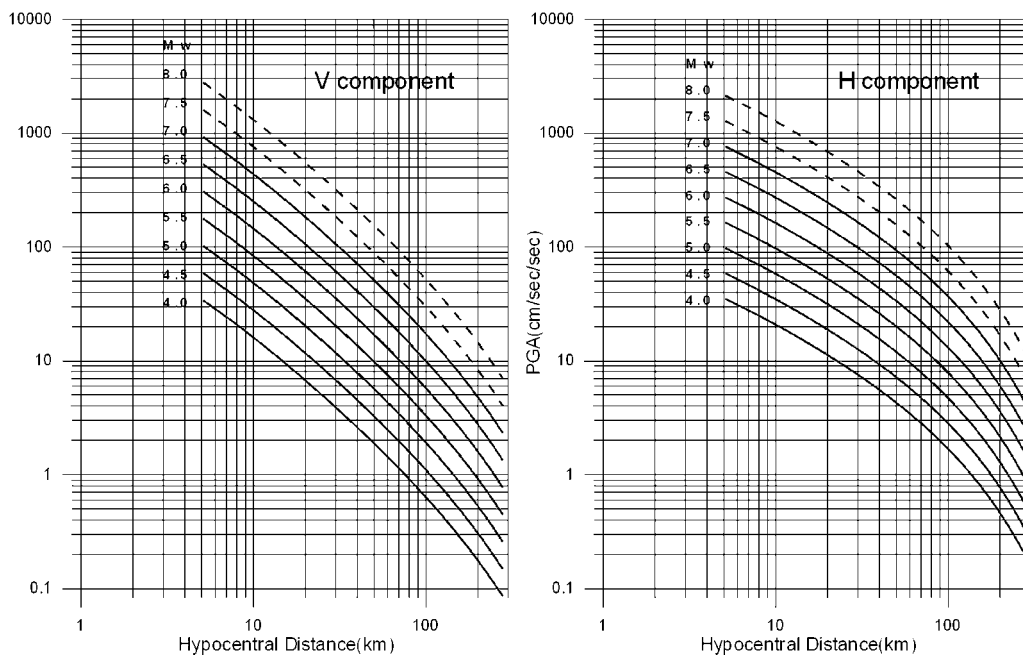


Figure 3. Median model predictions for the vertical and horizontal PGA.

Figure 5 shows the mean attenuation relationships of the horizontal PGA and PGV as a function of distance for moment magnitude M_w 6 for the whole Taiwan area and the three subareas (CHY, IWA, NTO). The figure shows that the average (TWN) curve lies close to the two non-CHY curves because the percentage of accelerograms used to derive attenuation relations at the CHY area accounts for only 17.5% (1382 of 7907). Additionally, note that both horizontal PGA and PGV at near-source distances have significantly higher values for earthquakes in the CHY area than in the other areas. At 10 km, both PGA and PGV are about four times larger for this area than for the other two areas and the average. This is because the CHY area in southwestern Taiwan is located on a thick alluvial plain. The other two areas in central and northeastern Taiwan are located on older geologic formations. This result is further supported later in this

article by the site residual contour maps of Figures 11 and 12, in which the maximum difference of site residuals between the CHY and NTO areas can reach up to 1.4 (i.e., $e^{1.4}$ equals to about 4).

The attenuation relationships of PGA and PGV for the NTO area in central Taiwan are compared with the observed data from the 1999 Chi-Chi earthquake (M_w 7.7) as shown in Figures 6 and 7, respectively. In Figure 7, the two highest PGV values, about 300 and 190 cm/sec, are from TCU068 (Shihkang station) and TCU052 stations, which are located in the hanging wall of the northern part of the Chelungpu fault. From the study of the Chelungpu fault by Wang *et al.* (2002), the reconstructed 3D fault plane not only dips to the east but also has a slight inclination to the south (about 10°). This means that the fault surface became shallower when it moved from south to north and finally was exposed at the

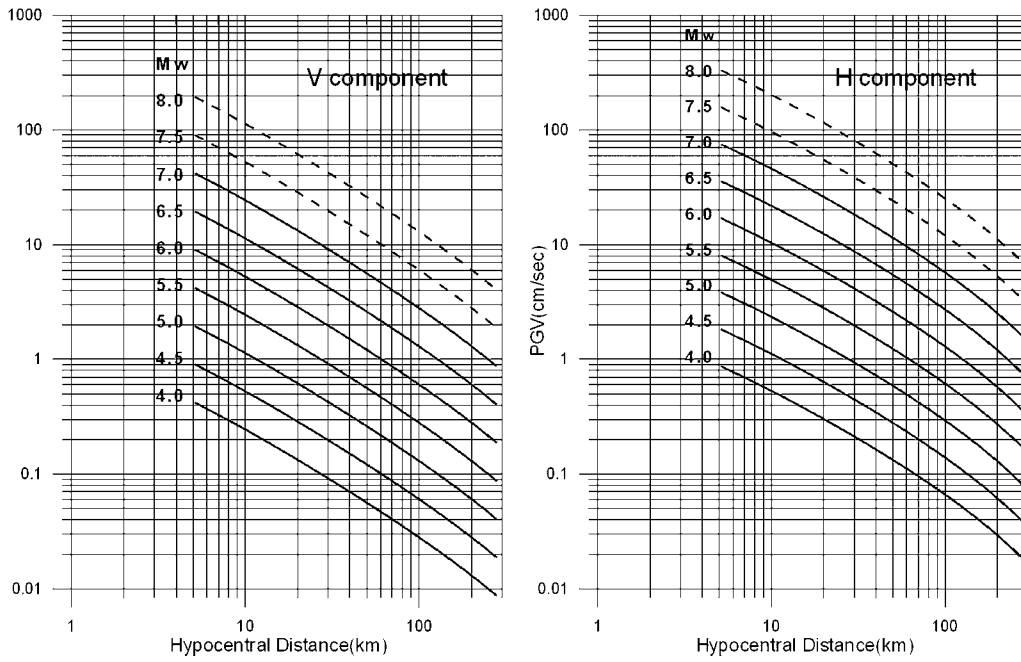


Figure 4. Median model predictions for the vertical and horizontal PGV.

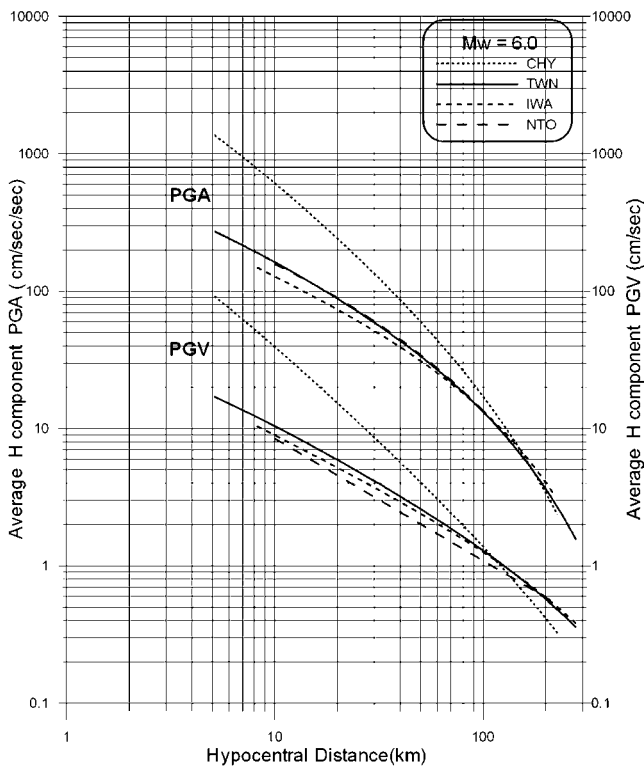


Figure 5. Median model predictions for the peak horizontal ground-motion parameters as a function of hypocentral distance for moment magnitude 6 in Taiwan and the three subareas (CHY, IWA, and NTO).

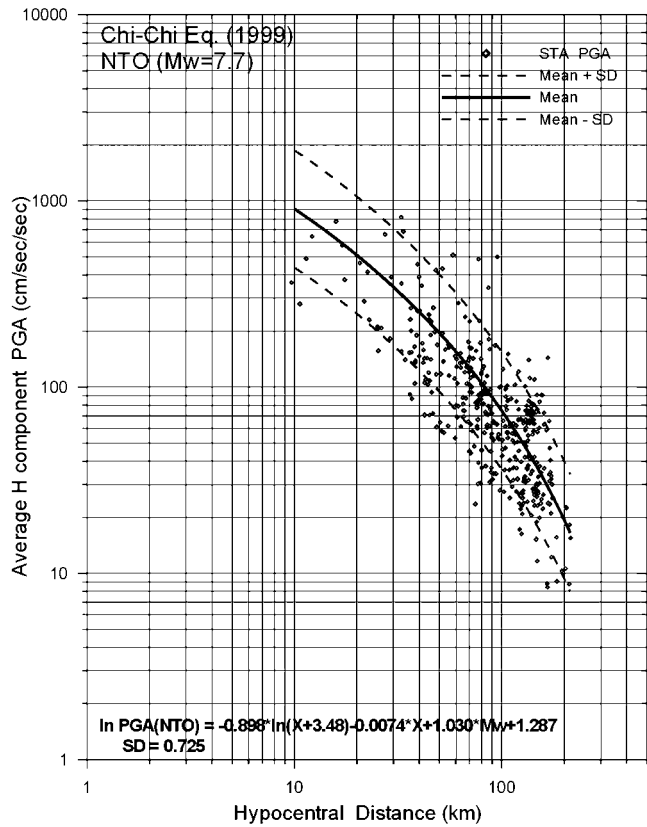


Figure 6. Comparison of the horizontal PGA data for the M_w 7.7 Chi-Chi earthquake with the corresponding median and median $\pm \sigma$ attenuation relationships listed in Table 2 for the NTO area.

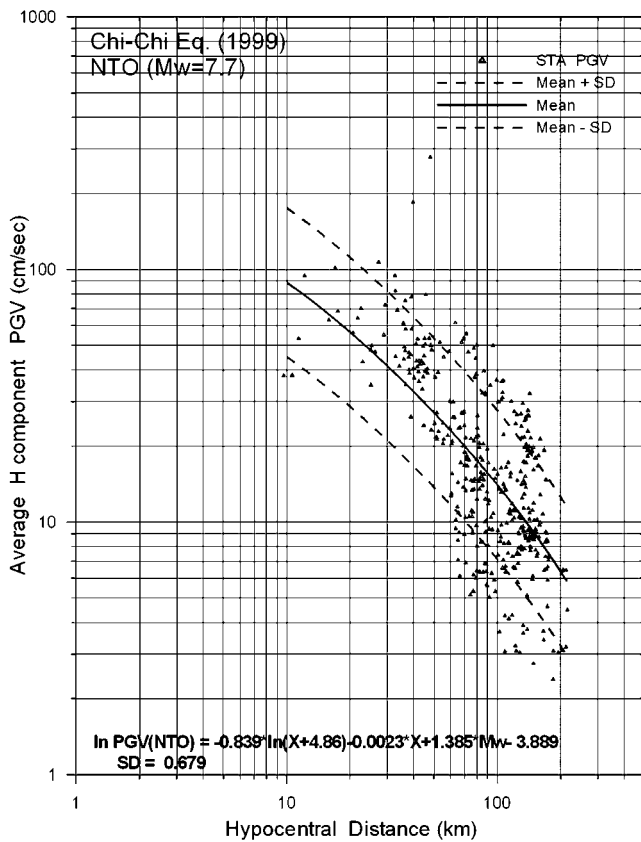


Figure 7. Comparison of the horizontal PGV data for the M_w 7.7 Chi-Chi earthquake with the corresponding median and median $\pm \sigma$ attenuation relationships listed in Table 2 for the NTO area.

surface along the banks of the Tachiahsi river in the Fengyuan-Shihkang area. This abnormal rupturing process might have resulted in unusually high PGV values. The figures show that the fit between the extrapolated attenuation curves and actual earthquake strong-motion data is close for both PGA and PGV.

We further compared our new PGA and PGV attenuation relationships with the strong-motion data of the 2003 Cheng-Kung earthquake (M_w 6.8) (Harvard CMT) which was located near the coast of southeastern Taiwan, as shown in Figures 8 and 9, respectively. (For location of the earthquake see Fig. 1). Most data from recordings were distributed within the range between plus and minus one standard deviation of the mean attenuation curve in Figure 8. After checking the horizontal PGV contour map, in Figure 9, we found that the two higher clusters of data, at hypocentral distances 40–50 km and 100–120 km, were located near Taitung city and Pingtung Valley, respectively. The lower cluster of data, at hypocentral distance 100–230 km, were scattered around northern Taiwan (see negative residual area marked on the site residual contour map of Fig. 12). The residual contour maps, especially for the PGV, have close correlation with the regional geology and topography of Taiwan, which will be discussed further later in this article. The

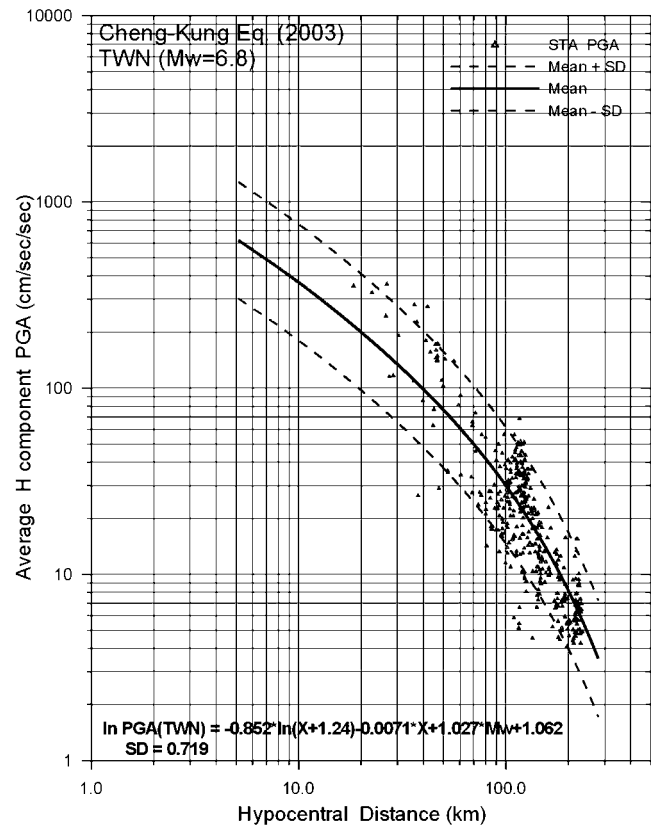


Figure 8. Comparison of the horizontal PGA data for the M_w 6.8 Cheng-Kung earthquake with the corresponding median and median $\pm \sigma$ attenuation relationships listed in Table 2 for the TWN area.

preceding test results show that our new attenuation relationships can be extrapolated to give reasonable estimates of strong ground motion from large earthquakes.

Figure 10 compares our new PGA attenuation relationship for M_w 6.5 with several attenuation models published before the Chi-Chi earthquake for the Taiwan region. (Loh, 1996; T. C. Shin, unpublished manuscript, 1998; Liu, 1999). Our new curve is very close to that of Loh (1996) but lower than the curve by Liu (1999) in near-field distances. This is because we added more than 3000 records from many large aftershocks located in central Taiwan (NTO area), a region of older geology. The curve of T. C. Shin (unpublished manuscript, 1998) differs from the others probably because he used the data from not only the crustal events but also from the subducting-plate events with focal depths ranging from 35 to 150 km.

Analysis of Site Residuals

Examination of the residuals for sites with different soil categories is a useful method for sets of records in which site information is not complete, and hence cannot be included explicitly within the equation (Abrahamson and Litehiser, 1989). Figures 11 and 12 show the site residual con-

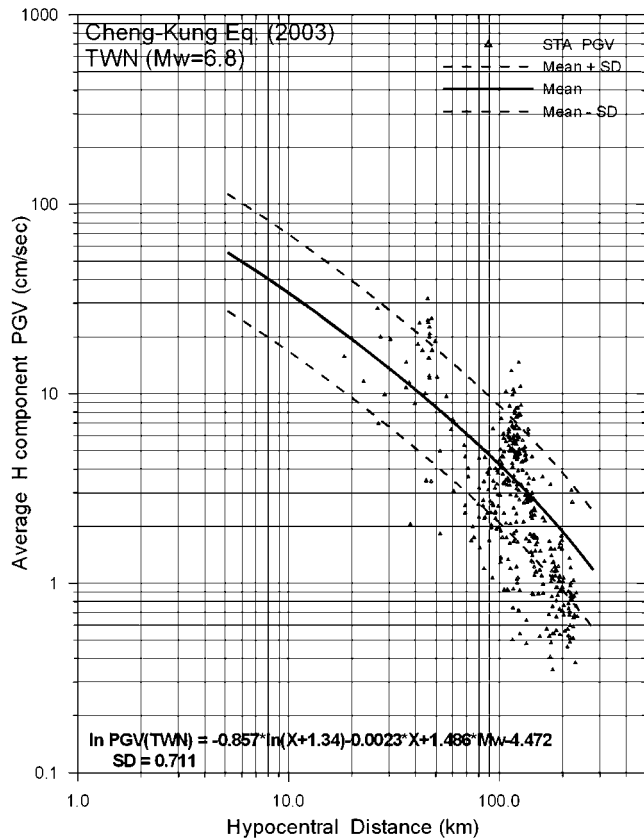


Figure 9. Comparison of the horizontal PGV data for the M_w 6.8 Cheng-Kung earthquake with the corresponding median and median $\pm \sigma$ attenuation relationships listed in Table 2 for the TWN area.

four maps for horizontal PGA and PGV, respectively, for Taiwan. The black, red, and blue lines in the map represent the contours of residual value (difference between logarithms of the observed and predicted ground motion) corresponding to 0.0, 0.2, and -0.2 , respectively. We have chosen these residual values as boundary lines because they are well constrained by the observed data.

From the contour maps of site residuals for the PGA and PGV data (Figs. 11 and 12), some regional features of ground-motion variations are highlighted for the mountain regions with negative residuals and for the Coastal Plain of western Taiwan with positive residuals, with general north-south trends. Other notable features in Figures 11 and 12 are: (1) The high PGA residual anomaly of Nanao area in northeastern Taiwan is related to high-density schist (Ho, 1984). (2) The high PGV residual anomalies of Pingtung Valley, Ilan Plain, and Taitung Longitudinal Valley are related to soft alluvium in these areas.

To understand the relation between the site residuals of ground-motion parameters and regional geology or topography, we plot the residual contours of horizontal PGV on the geologic and topographic maps of Taiwan, as shown in Figures 13 and 14, respectively. The black, red, and white lines in the map represent the residual values of 0.0, 0.2, and

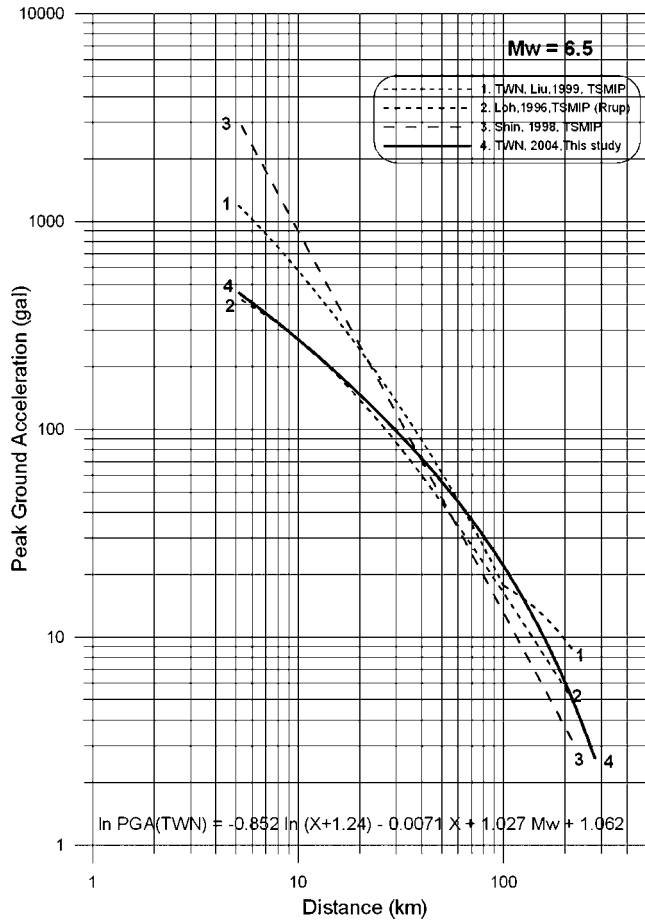


Figure 10. Comparison between some Pre-Chi-Chi attenuation models published for Taiwan.

-0.2 , respectively. In Figures 13 and 14, we can find that the black line (residual value equal to zero) matches closely with the boundary between the inner Western Foothills zone (belongs to the Miocene series) and the outer Western Foothills zone or the Flood Plain zone (belongs to the Holocene Alluvium, Pleistocene series, and Pliocene series). Accordingly, the positive PGV residuals cover areas like Taipei Basin, Changhua Plain, Chianan Plain, Pingtung Valley, Ilan plain, and Taitung Longitudinal Valley. Notably, most major metropolitan areas, including Taipei, Taoyuan, Hsinchu, Changhua, Tainan, Kaohsiung, Pingtung, Ilan, and Hualien are all in the positive residual areas that will experience amplification of ground motion. (For the location of cities, see Fig. 1.)

From the PGV residual contours, as shown in Figures 13 and 14, both the Pingtung Valley and Ilan Plain have high values. The Pingtung Valley in southern Taiwan is located between the lofty Central Range on the east and the low hills on the west. It is a sediment-filled trough, having a north-south length of 55 km and a east-west width averaging 20 km. This alluvial valley reveals anomalous evidence indicating that the Pingtung Valley is still actively subsiding. Voluminous detrital sediments are pouring into the Pingtung Valley

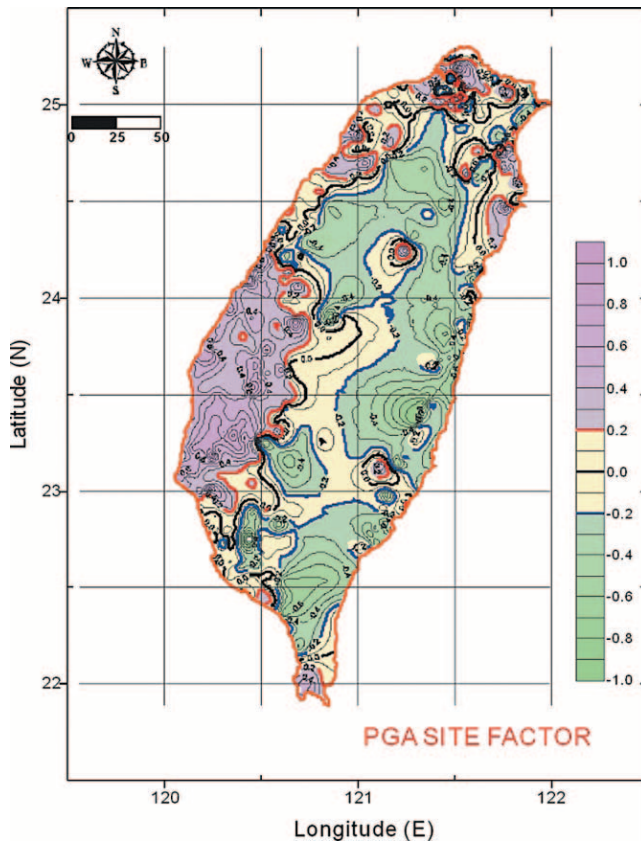


Figure 11. Distribution of the PGA residual values (difference between logarithms of observed and predicted accelerations) for the earthquakes of Table 1 by the color scale shown on figure. The black, red, and blue lines represent the contours of the residual values equal to 0.0, 0.2, and -0.2 , respectively.

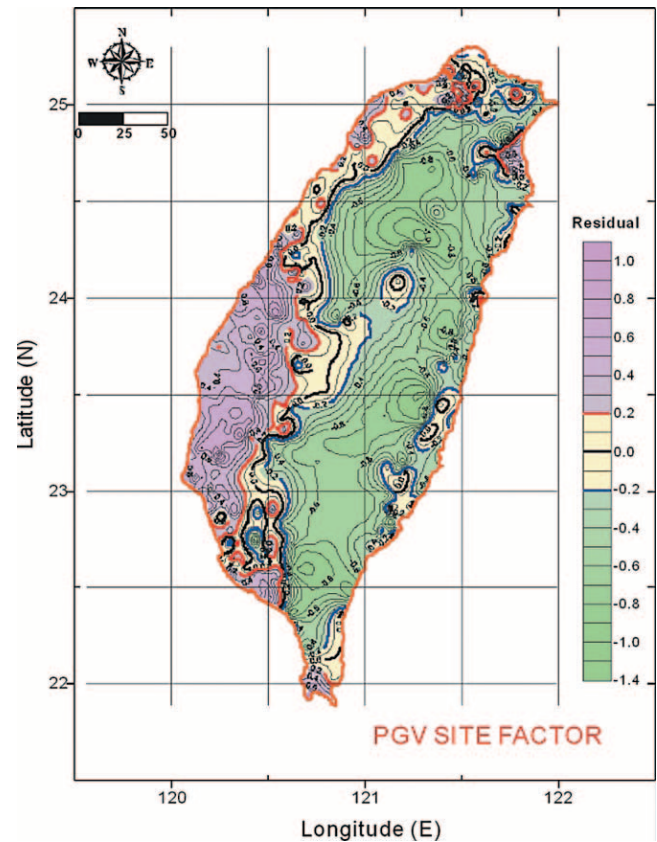


Figure 12. Distribution of PGV residual values (difference between logarithms of observed and predicted accelerations) for the earthquakes of Table 1 by the color scale shown on figure. The black, red, and blue lines represent the contours of the residual values equal to 0.0, 0.2, and -0.2 , respectively.

from the Central Range to the east and north. On the other hand, Ilan Plain is triangular on the northeastern coast, opening to the Okinawa Trough toward the east. The two other sides are fringed by high mountains composed mainly of Miocene to Paleogene slates. Tectonically, the Ilan Plain marks the western termination of the Okinawa Trough that extends from southern Japan toward the north ends of Taiwan. The extensional opening of the Okinawa Trough thus projects westward into Taiwan to form the Ilan Plain (Ho, 1982). Continuous subsidence caused by crustal extension has resulted in recent alluvial deposits in the Ilan Plain.

Additionally, the PGV residuals of the Taitung Longitudinal Valley are significantly higher than that of the Coastal Range. This is because the Taitung Longitudinal Valley contains thick alluvium and is fringed with an extensive series of alluvial fans mostly deposited by the streams draining the Central Range.

Discussion

Local site conditions at an accelerograph station can dramatically affect the strong motions recorded (Douglas,

2003). PGA and PGV are often useful for analysis of short period ($T < 0.3$ sec) and intermediate period ($T = 0.3 \sim 1$ sec) structures (Liu, 1999). Some studies though have found that shallow-soil sites have significantly higher ground motions than rock or stiff-soil sites and that rock and deep-soil sites have similar ground motion (Campbell 1981, 1989; Sabetta and Pugliese, 1987), although this is for PGA (a high-frequency parameter), which is less affected by local site conditions.

Up to now, the subsurface soil conditions of all free-field accelerograph stations in Taiwan has not been investigated in detail. Kuo (1992, 1993, 1994) used the 1991 Uniform Building Code (UBC) provisions (International Conference of Building Officials [ICBO], 1991) to classify 156 free-field strong-motion station series into four categories, namely S_1 , S_2 , S_3 , and S_4 (from hard to soft, respectively). Lee *et al.* (2001) conducted a more refined site classification by using surface geology from large-scale geologic maps, geomorphologic data, and borehole data. The site classes B, C, D, and E are comparable with S_B , S_C , S_D , and S_E in the 1997 UBC provisions and are used in the present classification system (Table 3).

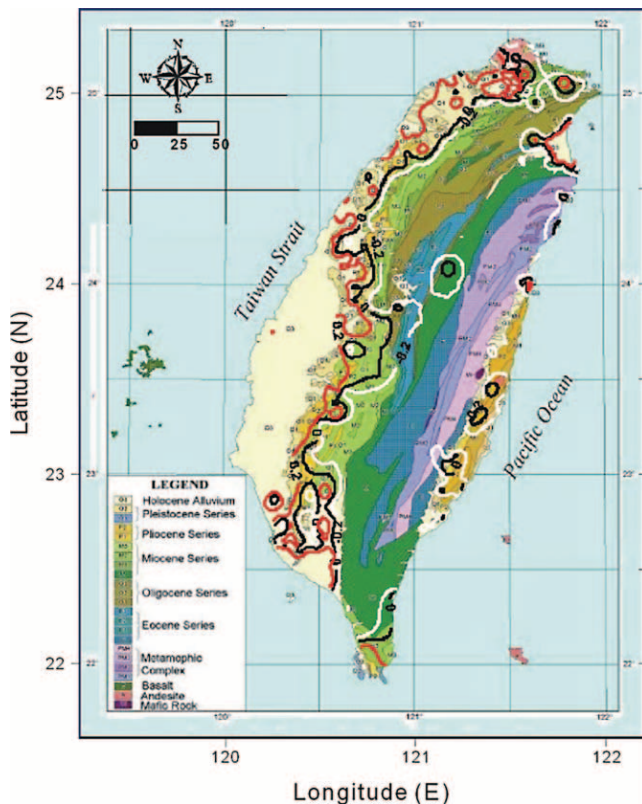


Figure 13. Distribution of PGV residual values (difference between logarithms of observed and predicted accelerations) after overlaying on the geologic map of Taiwan. The black, red, and white lines represent the contours of the residual values equal to 0.0, 0.2, and -0.2 , respectively. The base map was adopted from Lee *et al.* (2001).

According to the site classification made by Lee *et al.* (2001), as shown in Table 3, we divided the residuals of the vertical and horizontal components of PGA and PGV (difference between logarithms of observed and predicted ground motion), respectively, into three classes. Statistical results in Table 4 and Figure 15 show that most of the soil sites (class E) have positive residual values, especially for PGV; more than 40% of the stiff-soil sites (class D) and very dense soil or soft rock sites (class C) have intermediate residual values; most rock sites (class B) have negative residual values. It is clear from Figure 15 that (1) the PGV residual is more sensitive to the site class than the PGA residual, because the PGA is a high-frequency parameter that is less affected by local site conditions, and (2) the percentage of site classes C and D, as related to ground-motion residuals, are very similar.

Because the site class C (very dense soil) and site class D (stiff soil), as revealed by Figure 15, are similar in both PGA and PGV residuals, we propose to combine them into one class to simplify the site classification. In the meantime, geomorphology may also play an important role in site classification because a geomorphologic unit is often closely related to a geologic unit.

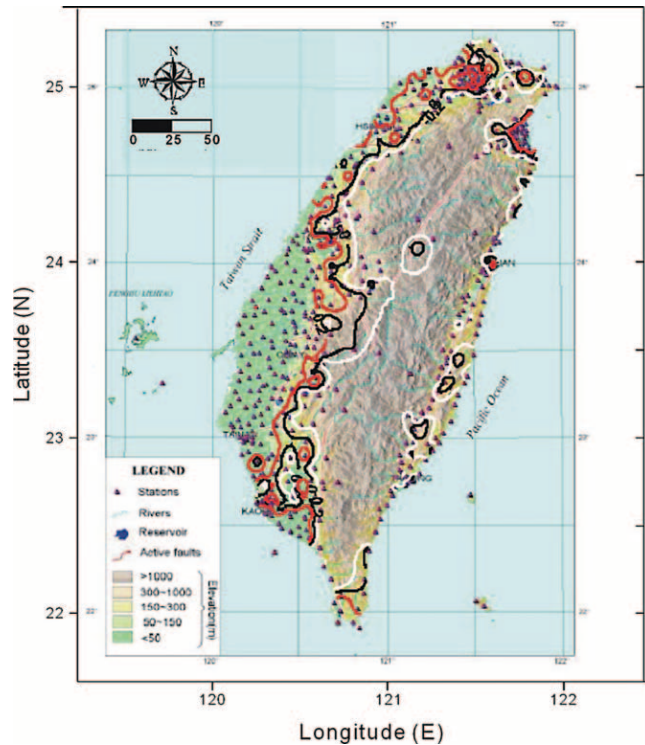


Figure 14. Distribution of PGV residual values (difference between logarithms of observed and predicted accelerations) after overlaying on the topographic map of Taiwan. The black, red, and white lines represent the contours of the residual values equal to 0.0, 0.2, and -0.2 , respectively. The base map was adopted from Lee *et al.* (2001).

We can find from Figure 14 that simplification of sites classification into three classes, that is class E (soft soils), C and D (dense and stiff soils), and B (rocks) will correspond to the flood plains at an elevation less than 50 m, terraces and tablelands at an elevation less than 1000 m, and high mountains (including some on limestone, igneous, and metamorphic rock sites at lower elevations), respectively.

Conclusions

From the preceding results and discussion, we can make the following conclusions.

1. For both PGA and PGV, the attenuation relationships for the vertical component decay faster with distance than for the horizontal component. In addition, the attenuation relationships of PGA decay faster with distance than that of PGV for the vertical component.
2. The stations in the CHY area in southwestern Taiwan have higher ground motion, either in PGA or PGV, at near-source distances than the other two areas, IWA in northeastern Taiwan and NTO in central Taiwan, and the

Table 3

Comparison between the 1997 UBC Provisions and the Simplified Site Classification Used in this Study (after Lee *et al.* 2001)

Site Class	Site Class Description of 1997 UBC Provisions	Site Class Description of Lee <i>et al.</i> (2001)
A	Hard-rock, eastern U.S. sites only, $\bar{V}_s > 1500$ (m/sec).	(Not used)
B	Rock, \bar{V}_s is 760–1500 (m/sec).	Miocene and older strata, and limestone, igneous rocks, and metamorphic rocks, etc.
C	Very dense soil and soft rock, \bar{V}_s is 360–760 (m/sec), undrained shear strength $u_s \geq 2000$ psf ($u_s \geq 100$ kPa) or $N \geq 50$ blows/ft	Pliocene and Pleistocene strata, and conglomerates, pyroclastic rocks, etc., and geomorphologic lateritic terraces
D	Stiff soils, \bar{V}_s is 180–360 (m/sec) stiff soil with undrained shear strength $1000 \text{ psf} \leq u_s \leq 2000 \text{ psf}$ ($50 \text{ kPa} \leq u_s \leq 100 \text{ kPa}$), or $15 \leq N \leq 50$ blows/ft	Late Pleistocene and Holocene strata, geomorphologic fluvial terrace, and, stiff clays and sandy soils with average SPT $N \geq 15$ in the upper 30 m.
E	Soft soils, profile with more than 10 ft (3 m) of soft clay defined as soil with plasticity index $PI > 20$, moisture content $w > 40\%$ and undrained shear strength $u_s < 1000$ psf (50 kPa), or $N < 15$ blows/ft.	Holocene deposits and fills, etc., with average SPT $N < 15$ in the upper 30m.
F	Soils requiring site-specific evaluations: 1. Soil vulnerable to potential failure or collapse under seismic loading: e.g., liquefiable soils, quick and highly sensitive clays, collapsible weakly cemented soils. 2. Peats and/or highly organic clays (10 ft [3 m] or thicker layer). 3. Very high plasticity clays (25 ft [8 m] or thicker layer with plasticity index > 75). 4. Very thick soft/medium stiff clays (120 ft [36 m] or thicker layer).	(This is not classified in the present study and will be studied in the future.)

The Provisions of 1997 National Earthquake Hazard Reduction Program (NEHRP) and 1997 UBC are similar.

Table 4

Number and Percentage (in Parentheses) of Sites Correlative with Site Residual

Site	Residual			Total
	$>0.2 \sigma$	$(-0.2 \sim 0.2) \sigma$	$<-0.2 \sigma$	
a. PGA V component				
B	20 (20)	43 (43)	37 (37)	100 (100)
C	27 (38)	28 (39)	16 (23)	71 (100)
D	107 (36)	131 (44)	62 (20)	300 (100)
E	90 (58)	52 (33)	14 (9)	156 (100)
b. PGV V component				
B	7 (7)	36 (36)	57 (57)	100 (100)
C	25 (35)	35 (49)	11 (16)	71 (100)
D	100 (33)	150 (50)	50 (17)	300 (100)
E	82 (53)	64 (41)	10 (6)	156 (100)
c. PGA H component				
B	14 (14)	35 (35)	51 (51)	100 (100)
C	25 (35)	30 (42)	16 (23)	71 (100)
D	98 (33)	119 (40)	83 (27)	300 (100)
E	102 (65)	40 (26)	14 (9)	156 (100)
d. PGV H component				
B	5 (5)	22 (22)	73 (73)	100 (100)
C	20 (28)	36 (51)	15 (21)	71 (100)
D	101 (34)	124 (41)	75 (25)	300 (100)
E	128 (82)	19 (12)	9 (6)	156 (100)

average for whole Taiwan. This is because the CHY area is located on a thick, recent alluvial plain.

3. The attenuation relationships developed for $M_w \leq 7$ can be extrapolated to make quick, reasonable estimates of strong motion for larger $M_w \geq 7$ earthquakes.

4. The ground-motion residual maps, especially for the PGV, show highly positive correlation with regional geology and topography. Note that there is a close correlation between the geology and topography of Taiwan.
5. The PGV residual contours reveal that Taipei Basin, Changhua Plain, Chianan Plain, Pingtung Valley, Ilan Plain, and Taitung Longitudinal Valley have high residual values. Consequently, most major metropolitan areas, including Taipei, Hsinchu, Changhua, Tainan, Kaohsiung, Pingtung, Ilan, and Hualien, are all in the high-residual areas that require special attention in the seismic design of structures.
6. We suggest simplifying site classification into three classes that are based on the geologic criteria by Lee *et al.* (2001), that is, class E for soft soils, class C and D for dense and stiff soils, and class B for rocks. These three site classes are mostly distributed, respectively, in the alluvial plains at an elevation less than 50 m, terraces and hills at an elevation less than 1000 m, and high mountainous areas, including some limestone, igneous, and metamorphic rock sites at lower elevations.

Acknowledgments

We thank the Central Weather Bureau and Institute of Earth Sciences, Academic Sinica of Taiwan for providing us with the strong-motion data. We are grateful to Dr. Joe Litehiser and an anonymous reviewer for their critical and helpful comments, which have led to significant improvement of the article. This research was supported by the National Science Council of the Republic of China under Grant NSC92-2625-Z-008-011.

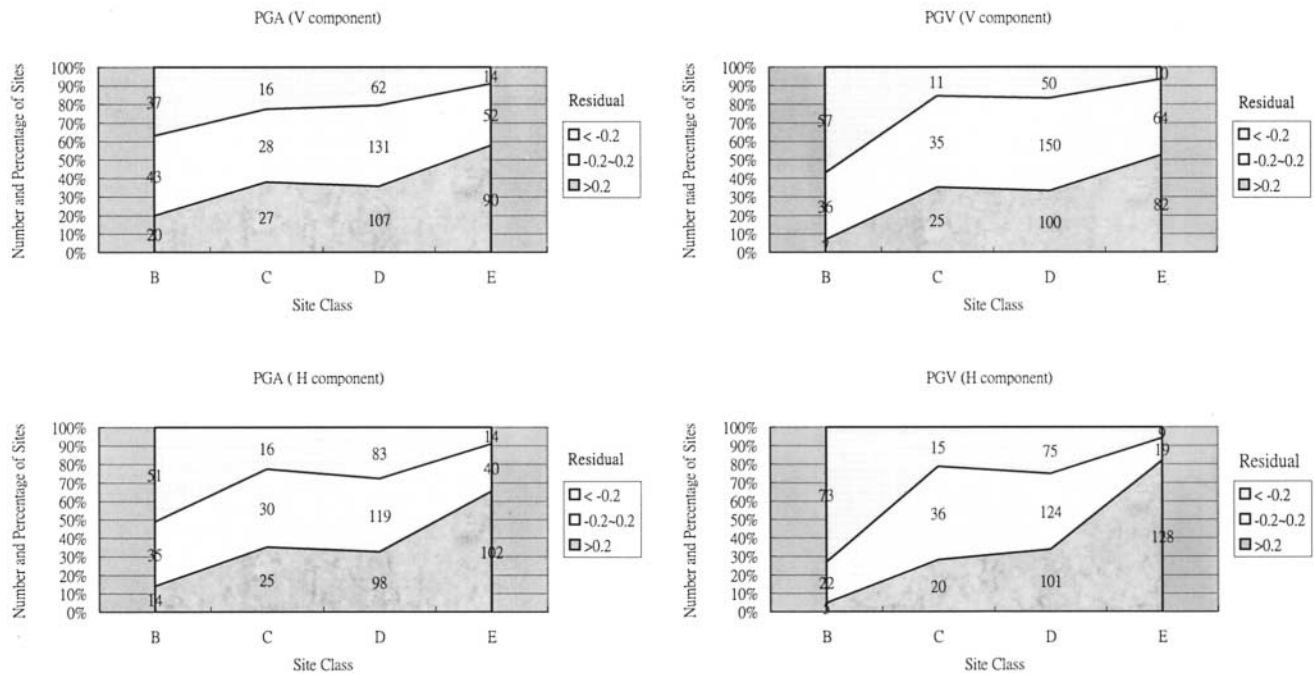


Figure 15. Statistics of ground-motion residuals of different site classifications. This diagram illustrates the number and percentage of different site classes in three residual ranges: $\sigma < -0.2$, $-0.2 \leq \sigma \leq 0.2$, $\sigma > 0.2$, as listed in Table 4.

References

- Abrahamson, N. A., and J. J. Litehiser (1989). Attenuation of vertical peak acceleration, *Bull. Seism. Soc. Am.* **79**, 549–580.
- Boore, D. M. (2001). Comparisons of ground motions from the 1991 Chi-Chi earthquake with empirical predictions largely based on data from California, *Bull. Seism. Soc. Am.* **91**, 1212–1217.
- Boore, D. M., W. B. Joyner, A. A. Oliver, III, and R. A. Page (1980). Peak acceleration, velocity and displacement from strong-motion records, *Bull. Seism. Soc. Am.* **70**, 305–321.
- Campbell, K. W. (1981). Near-source attenuation of peak horizontal acceleration, *Bull. Seism. Soc. Am.* **71**, 2039–2070.
- Campbell, K. W. (1989). The dependence of peak horizontal acceleration on magnitude, distance, and site effects for small-magnitude earthquakes in California and eastern North America, *Bull. Seism. Soc. Am.* **79**, 1311–1346.
- Campbell, K. W. (1997). Empirical near-source attenuation relationships for horizontal and vertical components of peak ground acceleration, peak ground velocity, and pseudo-absolute acceleration response spectra, *Seism. Res. Lett.* **68**, no. 1, 154–179.
- Campbell, K. W., and Y. Bozorgnia (2003). Updated near-source ground-motion (attenuation) relations for the horizontal and vertical components of peak ground motion acceleration and acceleration response spectra, *Bull. Seism. Soc. Am.* **93**, 314–331.
- Centroid Moment Tensor (CMT) Catalog, www.neic.cr.usgs.gov/neis/sopar/ (last accessed January 2005).
- Chang, T. Y., F. Cotton, and J. Angelier (2001). Seismic attenuation and peak ground acceleration in Taiwan, *Bull. Seism. Soc. Am.* **91**, 1229–1246.
- Douglas, J. (2003). Earthquake ground motion estimation using strong-motion records: a review of equations for the estimation of peak ground acceleration and response spectral ordinates, *Earth-Sci. Rev.* **61**, 43–104.
- Hanks, T. C., and H. Kanamori (1979). A moment magnitude scale, *J. Geophys. Res.* **84**, 2348–2350.
- Heaton, T. F., F. Tajima, and A. W. Mori (1986) Estimating ground motions using recorded accelerogram, *Surv. Geophys.* **8**, 25–83.
- Ho, C. S. (1982). Tectonic Evolution of Taiwan, *Explanatory Text of the Tectonic Map of Taiwan*, Central Geologic Survey, The Ministry of Economic Affairs, Taiwan, Republic of China.
- Ho, C. S. (1984). An Introduction to the Geology of Taiwan, *Explanatory Text of the Geology Map of Taiwan*, 2nd Ed., Central Geologic Survey, The Ministry of Economic Affairs, Taiwan, Republic of China.
- International Conference of Building Officials (1991) Uniform Building Code, International Conference of Building Officials, Whittier, California.
- Joyner, W. B., and D. M. Boore (1981). Peak horizontal acceleration and velocity from strong-motion records including record from the 1979 Imperial Valley, California, earthquake, *Bull. Seism. Soc. Am.* **71**, 2011–2038.
- Joyner, W. B., and D. M. Boore (1993). Method for regression analysis of strong-motion data, *Bull. Seism. Soc. Am.* **83**, 469–487.
- Kuo, K. W. (1992). The geological character of the CWB Strong Motion Network: Taipei area, Central Weather Bureau Open-file Rept. (in Chinese).
- Kuo, K. W. (1993). The geological character of the CWB Strong Motion Network: Taoyuan Hsinchu and Miaoli area, Central Weather Bureau Open-file Rept. (in Chinese).
- Kuo, K. W. (1994). The geological character of the CWB Strong Motion Network: Chianan area, Central Weather Bureau Open-file Rept. (in Chinese).
- Lee, C. T., C. T. Cheng, C. W. Liao, and Y. B. Tsai. (2001). Site classification of Taiwan free-field strong-motion stations, *Bull. Seism. Soc. Am.* **91**, 1283–1297.
- Liu, K. S. (1999). Attenuation relations for strong seismic ground motion in Taiwan, *Ph.D. Thesis*, National Central University, Chungli, Taiwan, 240 pp. (in Chinese with English abstract).
- Liu, K. S., T. C. Shin, W. H. K. Lee, and Y. B. Tsai (1993). Taiwan Strong Motion Instrumentation Program: the characteristics comparison of

- free-field accelerographs (in Chinese). *Meteorol. J. Central Weather Bureau* **39**, no. 3, 132–150.
- Liu, K. S., T. C. Shin, and Y. B. Tsai (1999). A free field strong motion network in Taiwan: TSMIP, *TAO* **10**, no. 2, 377–396.
- Loh, C. H. (1996). The parameters about the strong motion characteristics and the evaluation of seismic hazards, in *Guidelines of Aseismic Safety Evaluation and Retrofit for Telecommunication and Transportation Systems*, Nation Taiwan University Press, Taipei, Taiwan, 2–3 (in Chinese).
- Niazi, M., and Y. Bozorgnia (1991). Behavior of near-source peak horizontal and vertical ground motions over SMART-1 array, Taiwan, *Bull. Seism. Soc. Am.* **81**, 715–732.
- Reiter, L. (1991). *Earthquake Hazard Analysis: Issues and Insights*, Columbia University Press, New York, 254 pp.
- Sadigh, K., C. Y. Chang, J. A. Egan, F. Makdisi, and R. R. Youngs (1997). Attenuation relationships for shallow crustal earthquake based on California strong motion data, *Seism. Res. Lett.* **68**, no. 1, 180–189.
- Sabetta, F., and A. Pugliese (1987). Attenuation of peak horizontal acceleration and velocity from Italian strong-motion records, *Bull. Seism. Soc. Am.* **77**, 1491–1513.
- Shin, T. C. (1993). Progress summary of the Taiwan Strong Motion Instrumentation Program, *Symposium on the Taiwan Strong Motion Instrumentation Program*, Taipei, Taiwan, 28–29 December, 1–10 (in Chinese).
- Shin, T. C., and T. L. Teng (2001). An overview of the 1999 Chi-Chi, Taiwan, earthquake, *Bull. Seism. Soc. Am.* **91**, 895–913.
- Tsai, Y. B., and H. W. Huang (2000). Strong ground motion characteristics of the Chi-Chi, Taiwan earthquake of September 21, 1999, *Earthquake Eng. Eng. Seism.* **2**, 1–21.
- Wang, C. Y., C. L. Li, F. C. Su, M. T. Leu, M. S. Wu, S. H. Lai, and C. C. Chern (2002). Structural mapping of the Chi-Chi earthquake fault, Taiwan by seismic reflection methods, *TAO* **13**, no. 3, 211–226.
- Wu, Y. M., C. H. Chang, Y. B. Tsai, and T. C. Shin (1998). Improvement on earthquake location by using near-source P & S arrival and S-P time differences, *Symposium on the Taiwan Strong Motion Instrumentation III*, Chiayi, Taiwan, 10–11 June, 197–205 (in Chinese).
- Wu, Y. M., T. C. Shin, and C. H. Chang, (2001). Near real-time mapping of peak ground acceleration and peak ground velocity following a strong earthquake, *Bull. Seism. Soc. Am.* **91**, 1218–1228.

Kao Yuan Institute of Technology
Kaohsiung 821, Taiwan, Republic of China
(K.-S.L.)

Institute of Geophysics
National Central University
Chungli 320, Taiwan, Republic of China
(Y.-B.T.)

Manuscript received 31 August 2004.